energy&fuels

pubs.acs.org/EF Article

Fast Pyrolysis of Hemicelluloses into Short-Chain Acids: An Investigation on Concerted Mechanisms

Marion Carrier,* René Fournet, Baptiste Sirjean, Sam Amsbury, Yoselin Benitez Alfonso, Pierre-Yves Pontalier, and Anthony Bridgwater

Cite This: https://dx.doi.org/10.1021/acs.energyfuels.0c02901 Read Online

ACCESS | Metrics & More | Article Recommendations | Supporting Information

ABSTRACT: The nature of the main primary mechanisms involved in lignocellulosic fast pyrolysis is often assumed to be radical mechanisms. Here we demonstrate that thermal depolymerization of native hemicelluloses can undergo several primary and secondary concerted reactions leading to light oxygenates that can compete with radical mechanisms. To model these reactions at a microscopic level, we used high-level quantum calculations based on functional theory. In parallel, a set of experimental data was collected to confirm the main structural features of extracted and purified hemicelluloses and to describe chemical variations within fast pyrolysis products released from various hemicellulosic fractions at 823 K. In general, the barriers computed at 800 K for pericyclic reactions were found to be reasonably low competing with these of homolytic reactions. The critical role of hydrogen bonding and spatial arrangement on product distribution was clearly demonstrated, stabilizing effects depending greatly on temperature. We reported a useful data set of intrinsic kinetic parameters and a reaction network readily available to complete kinetic models for "primary" and "secondary" fast pyrolysis of hemicelluloses.

1. INTRODUCTION

The description and understanding of mechanisms and pathways are the cornerstone of any optimization process. Describing the sequential changes occurring at the molecular level and determining the sequence of reactions for biomass fast pyrolysis are key knowledge to control its kinetics and selectivity. This is best done by combining both experimental and theoretical approaches, with the theory providing a more comprehensive view of the complexity of events and backing up fundamentally some intricate chemical reactions. The application of these joint approaches can be of interest for complex processes such as biomass fast pyrolysis. A number of research studies have skillfully and successfully undertaken this challenge using quantum chemical methods and microkinetic modeling to study pyrolysis of natural polymers. When it comes to approach those complex systems the description of the initial molecules (i.e., reactants) becomes a critical stage as it determines the success of its modeling.[1] The complex nature of the lignocellulosic network prevents a straightforward, reliable definition and identification of the main influential structures.

For example, in the case of cellulose composed of a regular structure, a series of glucose units, we may be tempted not to scrutinize in more detail its degradation and therefore underestimate the intricacy of its degradation but also of its impact on the overall degradation of biomass. Although cellulose is best represented with a subunit of glucose, the role of hydroxyl groups, or more specifically the intramolecular H-bonding, and their "catalytic" role on the degradation of "glucose" into levoglucosan has recently been proven to be critical.[2] The presence of hydrogen bonding plays a critical role during the depolymerization facilitating the hydrogen-transfer reactions with the participation of lone-pair electrons. One of the most complete theoretical microkinetic models for the glucose fast pyrolysis was suggested by Vinu et al.[3] to model the bio-oil's composition. They have collated in total 99 key radical and concerted reactions previously described to model concentration profiles of typical polymeric chains and lower molecular weight products. By using continuous distribution kinetics, this kinetic model distinguishes itself from others considering the physical state of volatiles.

Other groups have chosen a semiempirical approach to describe kinetics patterns of cellulose fast pyrolysis based on the description of transport phenomena and lumped pyrolysis products.[4] Both approaches are important and complementary as they provide a global view of the pyrolysis process based on experimental observations on one hand[5,6] and a more intricate idea of the nature of chemical reactions.[1−3]

More recently, some of those modeling approaches have been applied to hemicelluloses pyrolysis,[7] and the validation of this applicability relies on the availability of rigorous experimental databases. As diverse as the lignin composition, the thermal behavior of hemicelluloses is currently being investigated as a large portion of its pyrolysis product remains unknown.[8] Although a quantified product distribution has been suggested for extracted and purified hemicelluloses;[9] most of the studies provide an extensive list of detected

Received: August 27, 2020
Revised: September 24, 2020
Published: September 28, 2020

organics, which is directly related to the wide abundance of plants cell walls. Typical hemicelluloses found within terrestrial plants are grouped in different classes: xyloglucans, xylans, mannans, glucomannans, and β-(1 → 3, 1 → 4)-glucans. The four former heterogeneous polysaccharides have a common feature, they are organized according a β-(1 → 4)-linked backbone with an equatorial configuration.[10]

Quality and quantity of hemicelluloses within harvestable lignocellulosic biomasses for the production of second biofuels generations can be found in the cell walls of grassy and woody plants.[10,11] Of interest are the following hemicelluloses: glucuronoarabinoxylan, galactoglucomannan, and β-(1 → 3, 1 → 4)-glucan that make up the largest hemicellulosic portion in those plants. Therefore, it is not surprising that a high number of 5C- and 6C-derived residues are detected when extracted hemicellulosic fractions composed of pentose (e.g., arabinose and xylose) and hexose (e.g., mannose and glucose) are pyrolyzed.[8] Other structures such as side chains and ferulic acid esters, important components of herbaceous hemicelluloses, can also be found and are suspected to be at the origin of a broad range of light oxygenates: acetic, propionic, and formic acids[8] and phenolics.[12,13]

When exposed to fast pyrolysis conditions, isolated hemicelluloses have led to the production of numerous compounds but only few studies[8,9] suggest the quantification of the condensable products normalized on a comparable basis while others[13−17] only provide a product distribution between detected products. Quantitative studies confirmed the detection of substantial levels of lower molecular weight compounds: 1-hydroxy-2-propanone (acetol) at 2.1−5.8 wt % on a bio-oil weight basis, formic acid at 21.1 wt %, acetic acid at 2.1−4.8 wt %, and propionic acid at 3.8 wt % to mention a few. When compared to other volatiles' composition derived from cellulose and lignin, concentrations of aliphatic carbons and carboxylic functions have been found to be higher.[8] The presence of those acids influences the acidic character of liquid fractions, which is partly at the origin of bio-oil's corrosiveness thus impacting piping and their storage. When stored, carboxylic acids react with alcohols through esterification reactions leading to the formation of water and ester and therefore changing the composition of bio-oil.[18] Recent findings indicate that the amount of monoprotic and polyprotic acids govern the overall acidity of bio-oils. By measuring the total acid number (TAN) of bio-oils, the authors have shown how increased concentrations of monoprotic acids (e.g., acetic and propionic acids) and diprotic acids (e.g., vanillic acid) contribute to the linear increase in TAN.[19] The typical range of TAN for fast pyrolysis bio-oil (FPBO) is 70−100 mg of KOH/g (according the ASTM D664) which is really high considering the maximum acid number of 0.50 mg of KOH/g required for conventional biodiesel.[20] This has a direct impact on the characteristics of transport fuels blends and blending ratios between FPBO and biodiesel, for example.[21]

The investigation undertaken here is meant to disclose the mechanistic origins of ones of the most detected short acids produced during the fast pyrolysis of isolated and purified hemicelluloses. The structure of glucuronoarabinaxylanan was identified as a surrogate for those hemicelluloses and experimentally processed. Simulations using quantum-chemistry methods based on density functional theory were used to identify the main pyrolysis pathways for the formation of those organic acids and to provide some explicit chemical rates of primary pyrolysis reactions.

2. EXPERIMENTAL METHODS

2.1. Extraction and Purification of Hemicelluloses. Three different samples of hemicelluloses have been used in this study: (i) HEMI-1, hemicelluloses extracted following the classical two-step sulfur-free soda pulping method from *Zea mays* leaves grown under controlled conditions in a greenhouse (RCS-1)[8] and purchased from IsoLife (Wageningen, The Netherlands); (ii) HEMI-2 and HEMI-3 have been also extracted using an alkali pulping method from harvested *Zea mays* (RCS-2) grown in natural soils (Gers, France). These two latter have been purified by ultrafiltration through a hollow fiber poly(ether sulfone) membrane with a molecular weight cutoff of 30 kDa applying a low and high retentate flow rates (see details in the Supporting Information). The ultrafiltration of hydrolyzates was found to be beneficial for the removal of inorganics that could have been introduced earlier via the alkali extraction as indicated by the substantial differences between ash contents of simply extracted hemicelluloses (Hemi-1) and purified hemicelluloses (Hemi-2 and Hemi-3). Both applications of longer ethanol extraction time and higher retentate flow rate during the ultrafiltration were favorable to reduce the ash content of isolated hemicelluloses (Hemi-2; Table 1).

Table 1. Ultimate Analysis of Extracted Hemicelluloses in wt %

type	C[a]	H[a]	N[a]	S[a]	O[b]	ash
RCS-1[8]	41.6	5.65	1.31	0.06		
RCS-2	41.9	5.68	2.14	0	40.94	9.37
Hemi-1[8]	34.6	5.35	0.75	0	43.90	15.4
Hemi-2	37.9	5.07	0.77	0	53.44	2.82
Hemi-3	39.7	5.66	0.70	0	50.61	3.33

[a]Method ASTM D 5291-02; calibration standard: Sulphanilamide. [b]O content determined by difference.

2.2. Characterization of Hemicelluloses. An enzyme-linked immunosorbent assay (ELISA) using spectrophotometry has been used to describe the different hemicellulosic fractions. Raw feedstocks and the extracted hemicelluloses have been analyzed by using specific monoclonal antibodies (mAbs) to reveal epitope complexity and heterogeneity. Glycome profiles were obtained by probing immobilized samples with a broad range of mAbs that were selected based on their capacity to specifically bind to a structural motif of a polysaccharide (see Table S1 for the complete list of mAbs and corresponding epitopes). After further purification and incubation, the performance of binding reactions between antibodies and polysaccharides was revealed in ELISAs by measuring absorbance at 450 nm (see the Supporting Information for more details).

2.3. Fast Pyrolysis of Hemicelluloses and Volatiles Analyses. The isolated hemicelluloses were pyrolyzed at 550 °C under the heating rate of 452 °C s^{-1} using a CDS 5200 micropyrolyser (Py-GC/MS) supplied by CDS Analytical. The hot volatiles were analyzed using a PerkinElmer gas chromatograph−mass spectrometer/flame ionization detector system (GC-MS/FID, Clarus 680-Clarus 600S). Products were identified using only mass spectrometry (MS). The MS spectra obtained were compared to the standard spectra of compounds found in the NIST library (2017). The retention time of products and order of separation were checked against those of pure standards found in previous studies using the same system.[8,22] More details on the fast pyrolysis and identification can be found elsewhere.[8]

3. COMPUTATIONAL DETAILS

Although the structural variability in hemicelluloses is really broad,[10] a subunit representative of a glucuronoarabinoxylanan (Figure 1) has been selected. Present in a large amount within

https://dx.doi.org/10.1021/acs.energyfuels.0c02901
Energy Fuels XXXX, XXX, XXX−XXX

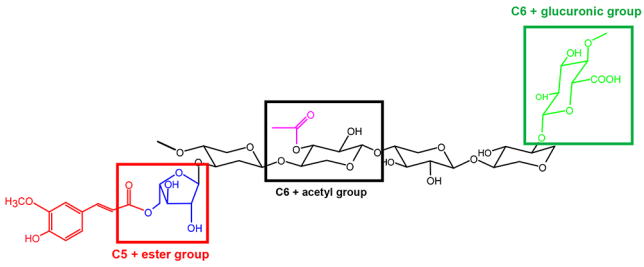

Figure 1. Representation of a hemicellulosic fragment, a glucuronoarabinoxylanan composed of a D-xylose unit (β1−4 equatorial position), α-1,3-L-arabinose with ferulic acid, and acetyl and glucuronic acid groups.[10]

the plant cell wall of grassy biomass, this type of hemicellulose was subdivided in three systems for the sake of ease of calculation.

Identification and energy optimization of the reactants' structure have been carried out using the quantum-chemistry package Gaussian 09.[23] For all substructures considered in this work (Figure 1), the first step has consisted of finding the lowest energy conformer by performing relaxed scans for all internal rotations existing in the hemicellulosic fragment of Figure 1. For instance, in the C6+acetyl group, the polymeric structure connected to this fragment has been replaced in the model molecule by a methyl group (Figure 2). In this case, internal rotation of the CH_3O-fragment has not been taking into account since this rotation does not exist in the hemicellulose. Indeed, hemicelluloses are characterized by a β-(1 → 4)-linked backbone with an equatorial configuration at C1 and C4 thus maintaining the methoxy groups in the equatorial position. These scans have been done at the B3LYP/6-31+G(d,p)[24] level of theory. Whenever a new conformer of low energy was found, geometry optimization and frequency calculations were performed, and new relaxed scans were done to ensure that there was no lower energy structure. Otherwise, the procedure was repeated until the global minimum was found. The same procedure has been used for transition states even if the lower energy conformers are easier to find, due to numerous internal rotations frozen. At this stage, frequency calculations were used to check that transition states corresponding to first order saddle points (only one imaginary frequency). CBS-QB3[25] calculations were carried out for all of the lowest energy conformers found previously. This level of theory allows a greater accuracy in energy calculations but dramatically increases the computational time because of the use of coupled cluster (CCSD(T)) theory in energy calculations. In CBS-QB3 calculations, geometry optimizations and frequency calculations were performed at the B3LYP/6-311G(d,p) level of theory. Single-point calculations (CCSD(T), MP4, and MP2) were performed on the optimized geometry.

Rate coefficients, $k(T)$, for all of the reactions investigated were obtained from the canonical transition state theory (eq 1):

$$k(T) = L\frac{k_B T}{h}\frac{Q_{TS}(T)}{Q_R(T)}\exp\left[-\frac{V^{\ddagger}}{RT}\right] \quad (1)$$

where k_B is Boltzmann's constant, h is Planck's constant, T the temperature and $V^{\ddagger}$, the classical barrier height. $Q_{TS}(T)$ and $Q_R(T)$ are the partition function calculated, respectively, for the transition state (TS) and the reactant (R). L is the statistical factor (eq 2) defined as

$$L = \frac{\sigma_R n_{TS}}{\sigma_{TS} n_R} \quad (2)$$

σ_R and σ_{TS} are the external symmetry of respectively the reactant and the transition state, while n_R and n_{TS} correspond to their number of optical isomers.

The transmission coefficient κ was computed from a one-dimensional asymmetric Eckart potential[26] to consider the tunneling effect. Partition functions were computed using statistical thermodynamics implemented in the THERMROT program.[27] Internal rotations were treated as hindered rotors rather than harmonic oscillators by means of a modified one-dimensional hindered rotor formalism.[28]

Finally, rate coefficients are deduced from eq 3 and fitted over the temperature range of 500−600 °C, from a three parameters Arrhenius expression (eq 3):

$$k_\infty(T) = AT^n e^{-E/RT} \quad (3)$$

where k_∞ is the rate of reaction, A is the pre-exponential factor, T is the temperature, n is the order of the reaction, R is the universal gas constant, and E is the apparent activation energy.

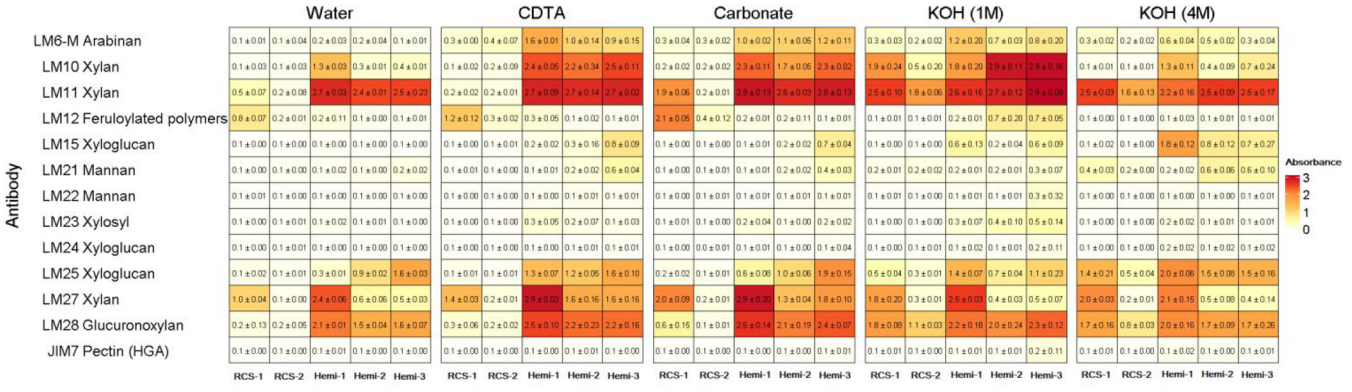

Figure 2. Spectrophotometric color determination of ELISAs for the raw feedstocks (RCS-1 and RCS-2) and different hemicellulosic fractions (Hemi-1, Hemi-2, and Hemi-3), measured absorbance (arbitrary units) at 450 nm after that antibodies react specifically to plate-bound hemicellulosic motifs.

https://dx.doi.org/10.1021/acs.energyfuels.0c02901
Energy Fuels XXXX, XXX, XXX−XXX

4. RESULTS AND DISCUSSION

4.1. Description of Hemicelluloses. Structural motifs of hemicelluloses, such as xylan at different degrees of substitution (LM10, LM11, and LM27), glucuronoxylans (LM27 and LM28), xyloglucans (LM15, LM24, and LM25), and arabinans ((LM6/BR12), typically known to constitute the large portions of grassy-derived hemicelluloses[29] have been detected.

Molecular probes have been used to reveal more details about the structural motifs of raw biomass cell wall and extracted polymers (Figure 2) in order to identify structural motifs for the hemicellulosic fragments (Figure 1).

Depending on the extraction method applied (Water, Carbonate, CDTA, 1M KOH or 4M KOH), the raw *Zea mays* feedstocks contain different structural arrangements. The RCS-1 grown in a controlled area and made of leaves shows high binding to a larger range of antibodies (LM11, LM12, LM27, and LM28) indicating higher proportions of xylan/glucuronoxylans than RCS-2. It appears obvious that the presence of ferulic acid units (binding with LM12) is significantly affected by different extraction treatments.

Structural differences within raw materials are also expressed among their respective hemicellulosic extracts. Hemi-1 shows high binding with both LM15 and LM27 confirming high proportions of xylan/glucuronoxylan and xyloglucan motifs.

The fact that the absorbance decreased for more drastic dissolution mediums in the case of purified hemicelluloses (Hemi-2 and Hemi-3) may indicate that both ethanol extraction and ultrafiltration stages have contributed to the decrease in the portion of glucuronoxylan motifs.

The case of arabinans, bound by LM6, is interesting. Those polysaccharides are sometimes excluded from the hemicellulosic group and classified as pectin molecules as they do not share the equatorial β-(1 4)-linked backbone structure. In this study, we showed that arabinan side chains (high absorbance for LM6/BR12) were present although the lack of homogalacturonan, indicated by the absence of JIM7 binding suggests that there is no pectin contamination.

Finally, with the detection of ferulic acid units (binding with LM12) mainly present in the purified hemicellulosic fractions, this molecular screening has confirmed the presence of three subunits: xylan/glucuronoxylan, xyloglucan, and ferulic acids (Figure 1).

4.2. Low Molecular Weight Compounds Detection. The three isolated hemicellulosic fractions were converted under fast pyrolysis (at 550 °C exposed to a heating rate of 425 °C/s; Figure 3). A previous study has indicated that the alkali-extracted hemicelluloses yielded a large amount of char, 40 wt %,[8] indicating the propensity of the hemicellulosic polymer and its pyrolysis products to promote the char formation.

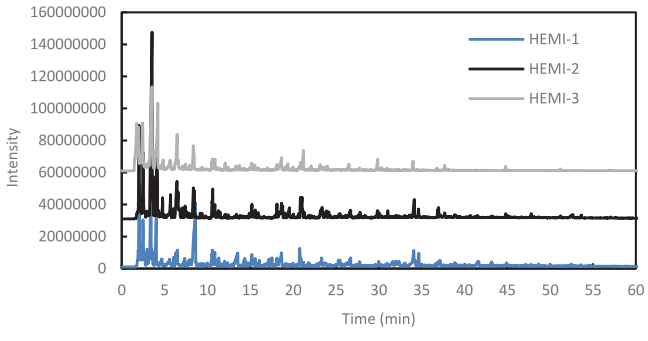

Figure 3. GC-FID chromatograms of fast-pyrolysis products from the isolated hemicellulosic fractions.

Despite several structural changes undergone by hemicelluloses during their alkali extraction reported,[11] the main motifs have been retained within the native structure (see section 4.1).

The previous screening of condensates evolved from the fast pyrolysis of Hemi-1 (Table S2) has revealed that condensate-based products include nonaromatic oxygenates (12.88 with 8.56 wt % of short acids and 3.41 wt % of ketones), heterocyclic compounds (1.44 wt % with 1.36% of furans and 0.07 wt % of pyrans), aromatic compounds (0.33 wt % including a main "lignin-derived" products fraction of 0.245 wt %), and anhydrosugars (1.91 wt %) making up a weight portion of 16% of the wet bio-oil.

The use of the micropyrolyzer has allowed the identification of commonly detected LMW compounds within hot pyrolysis volatiles: acetic acid, 1-hydroxy-2-propanone (acetol), and 2-furaldehyde (furfural) to name a few (Table S3). This result is in line with the presence of high proportions of xylan previously detected (section 4.1) and corroborates some proposed primary degradation patterns of xylan.[30]

The purification of hydrolyzates by ultrafiltration removing a substantial content of inorganics before the recovery of hemicelluloses has definitively changed the chemical composition of primary products: the production of acetic acid increasing by an order of 3 while that of furfural is decreased by at least an order of 10 (Table S3). These trends can be attributed to the structural changes between the hemicellulosic feedstocks but most probably to the presence of high ash content in the nonpurified hemicelluloses. The chemical composition was previously reported and displayed large concentrations in Na and Ca[8], with those alkalis favoring the formation of furfural at 550 °C.

We notice that a range of heavier molecular weight compounds (e.g., phenol, guaiacol, and *o*-cresol) often attributed to the presence of lignin has been also detected (Table S3). This finding suggests a more extensive list of initially detected lignin-derived compounds than suggested by Werner et al.[13] and Wang et al.[31] and confirming further the cross-linked bonding of hemicelluloses with lignin.

4.3. Modeled Mechanisms. It is important to remember that the focus of this study was to suggest some relevant mechanisms leading to the formation of low molecular weight oxygenates in particular carboxylic acids from the fast pyrolysis of hemicelluloses.

Although it is quite difficult to discriminate between radical and concerted mechanisms, a number of experimental[32−36] and theoretical studies have provided evidence that support the occurrence of concerted mechanisms during the primary degradation stage of biomass fast pyrolysis.

In the following paragraphs, concerted reactions are used to explain "primary" fragmentation reactions during the fast pyrolysis of hemicelluloses and then propose reactional alternative to speculated radical mechanisms.[37]

4.3.1. C6 + Acetyl Group. It is quite well-known that xylans are the major noncellulosic polysaccharide in primary walls of grassy biomass and are often acetylated to various degrees.[10] This has been taken into account in our study by representing the "C6 + acetyl group" system as a combination of a xylose unit combined with an acetyl group attached to the O-3

https://dx.doi.org/10.1021/acs.energyfuels.0c02901
Energy Fuels XXXX, XXX, XXX−XXX

position of xylose (Figure 1). The four configurations chosen to represent this system differ in the position of the acetyl and hydroxyl groups with respect to the cycle that is in axial or equatorial position (Figure 4). To avoid prohibitive calculation

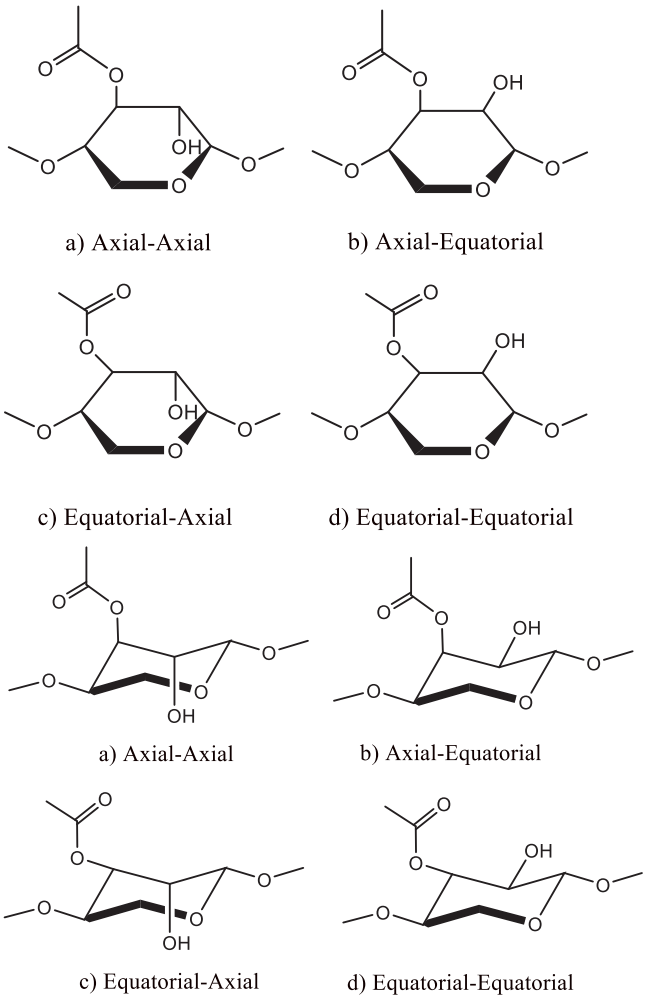

Figure 4. Representation of the four possible configurations of the "C6+acetyl" subunit.

times, the saccharide units within the hemicelluloses fragment (Figure 1) have been replaced by CH3. Moreover, the equatorial positions of the resulting CH3-O groups (Figure 4) have been "frozen", in order to be consistent with the position of saccharide units that forms the backbone of hemicelluloses.

The lowest energy conformers have been obtained for these four configurations after geometry optimization calculations and running a relaxed scan of the same optimized geometry (including both hydroxyl and acetyl substituents). The resulting zero-point energy differences relative to the lowest energy molecule were computed at 0 K (Table 2).

Table 2. Relative Difference between Zero-Point Energies of the Four Molecules for the "C6+Acetyl" Subunit, Relative to the Lowest Energy (A-A)[a]

ΔE (kcal mol^{-1})	A-A	A-E	E-A	E-E
B3LYP	0	1.52	1.19	0.32
CBS-QB3	0	2.12	1.43	1.54

[a]A and E denote axial and equatorial positions as depicted in Figure 3.

Independently from the method used, the lowest energy conformer corresponds to the acetyl and the hydroxyl groups in axial position. Also, the energy differences observed between the four isomers remain small (less than 2 kcal/mol). For each configuration, the formation of further hydrogen bonds were observed: (i) between the hydrogen atom of the hydroxyl group and lone electron pairs of the acetyl function and/or (ii) between the hydrogen atom connected to the carbon atom bearing the acetyl function and lone electron pairs of the O atom of the carbonyl group. These intramolecular interactions have a stabilizing effect and lower the energy of each structure in gas phase.[38] Although, we found that differences between energies computed using CBS-QB3 method for every conformers are really close to those obtained with the B3LYP method (Table 2), there is an exception with the E-E isomer, for which a different trend is observed: the B3LYP energy for E-E isomer, 0.32 kcal/mol, is significantly lower than the CBS-QB3 energy, 1.54 kcal/mol, questioning the accuracy of the B3LYP method.

When investigating the conversion of the "C6+acetyl" system, the structure of optimized conformations (a−d in Figure 3) stabilized by hydrogen bondings strongly suggests the occurrence of pericyclic reactions (Figure 5). The unimolecular pathways (1 and 2) proceed through a six-center concerted reaction with the formation of acetic acid.

Two hydrogen atoms can be transferred from the C6+acetyl group to form acetic acid (reactions (1) and (2), Figure 5). Although the transformation of E-A and E-E conformers can happen via both pathways 1 and 2, this was not the case for the A-A and A-E conformers (Figures 3a,b). In the case of the A-A configuration, the position of the acetyl group and the hydrogen atom on opposite sides of the ring prevents pathway 2 from happening, while both pericyclic reactions cannot occur in the case of A-E isomer. The energy barriers obtained for isomers A-A, E-A, and E-E at the two levels of theory: B3LYP/6-31+G(d,p) and CBS-QB3 are summarized in Table 3.

Among the possible reactions, the pericyclic reaction (1) involving the E-E conformer and yielding to primary byproducts, a pyran compound and acetic acid, displayed the lowest barriers independently from the two levels of calculation. The six-center cyclic transition states obtained (Figure 6) show close activation barriers of 43.02 and 45.15 kcal/mol for B3LYP and 50.16 and 52.45 kcal/mol for CBS-SB3. For the A-A isomer, only one TS can be obtained as previously discussed. Their corresponding energy barriers of 49.31 and 56.05 kcal/mol respectively for B3LYP and CBS-QB3 are greater than those calculated for the E-E isomer, which can be, partly, explained by the ring inversion occurring during the formation of the transition state. Figure 7 shows the boat conformation of the TS, which is due to the rotation of the hydroxyl group from an axial to an equatorial position.

This rotation allows the formation of the double bond but also leads to a TS from boat to chair conformation. This result is questionable because the initial molecule is a polymer and if the truncated structure of the model molecule permits such a motion, it is unlikely to happen as the polymer chain mobility should be drastically reduced. Two transition states have been found for the E-A isomer, with energy barriers of 69.07 and 57.16 kcal/mol for reactions (1) and (2), respectively, at the CBS-QB3 level of theory. The first value is particularly high and can be explained by the geometric constraints induced by the nascent π bond in the ring, in connection with the specific

https://dx.doi.org/10.1021/acs.energyfuels.0c02901
Energy Fuels XXXX, XXX, XXX−XXX

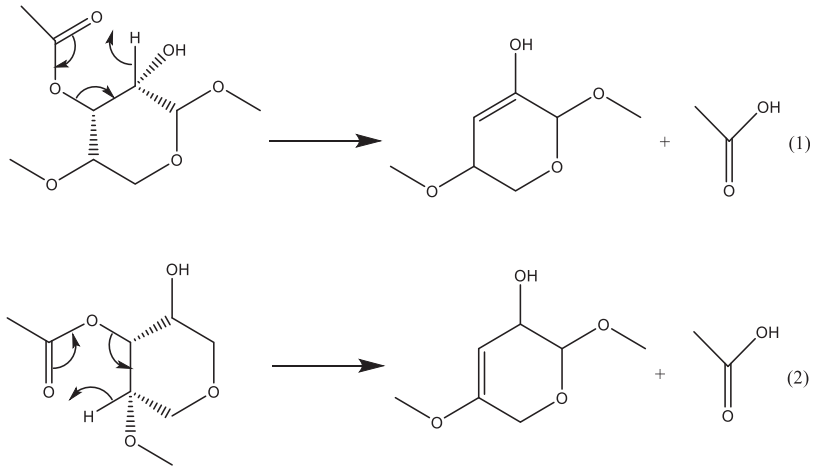

Figure 5. Formation of acetic acid by pericyclic reaction from the "C6+acetyl" subunit.

Table 3. Energies Barriers (at 0 K) Including Zero-Point Energy to Overcome for the Formation of Acetic Acid from the C6+Acetyl Subunit[a]

E_a (kcal/mol)	reaction	A-A	E-A	E-E
B3LYP	(1)	49.31	61.93	43.02
	(2)		51.13	45.15
CBS-QB3	(1)	56.05	69.07	50.16
	(2)		57.16	52.45

[a]A and E denote axial and equatorial position and are related to Figure 5.

position of the hydroxyl group and the H atom in the cycle (Figure 8).

Overall, the level of the energy barrier of 50.16 kcal/mol (CBS-QB3) found for the pericyclic reaction leading to the formation of acetic acid from the decomposition of the "C6-acetyl" group remains largely lower than that corresponding to the homolytic dissociation of acetyl groups from 2-O-acetyl-xylopyranose, 91.6 kcal/mol at the same level of theory.

From a purely energy point of view, this study showed that acetic acid can be formed through pericyclic reactions from the C6+acetyl system and that these reactions are facilitated when both acetyl and hydroxyl substituents are in equatorial position (E-E isomer). Previous experimental results obtained at a larger scale indicated the formation of acetic acid as a main fast pyrolysis product, up to 4.8 wt %, and few pyran compounds within the condensates (Table S2).[8] However, the screening of "primary" hot volatiles from the fast pyrolysis of hemicellulosic fractions using the Py-GC/MS technique revealed the constant detection of the acid and the absence of pyran-derived products (Table S3).

In addition to the barrier heights computed at the CBS-QB3 level of theory, we deduced the rate constants, based on the methodology described in section 3. Table 4 gives the reaction rate coefficients corresponding to eq 3, while Figure 9 displays rate constants against temperature range between 500 and 1500 K.

For temperatures above 650 K, the A-A conformer has the highest rate constant while it is the conformer having the acetyl and hydroxyl groups in equatorial position (E-E(1)) which leads to the fastest rate of formation of acetic acid below this temperature. This change can be explained by a competition between energetic (energy barrier) and entropic effects. If the

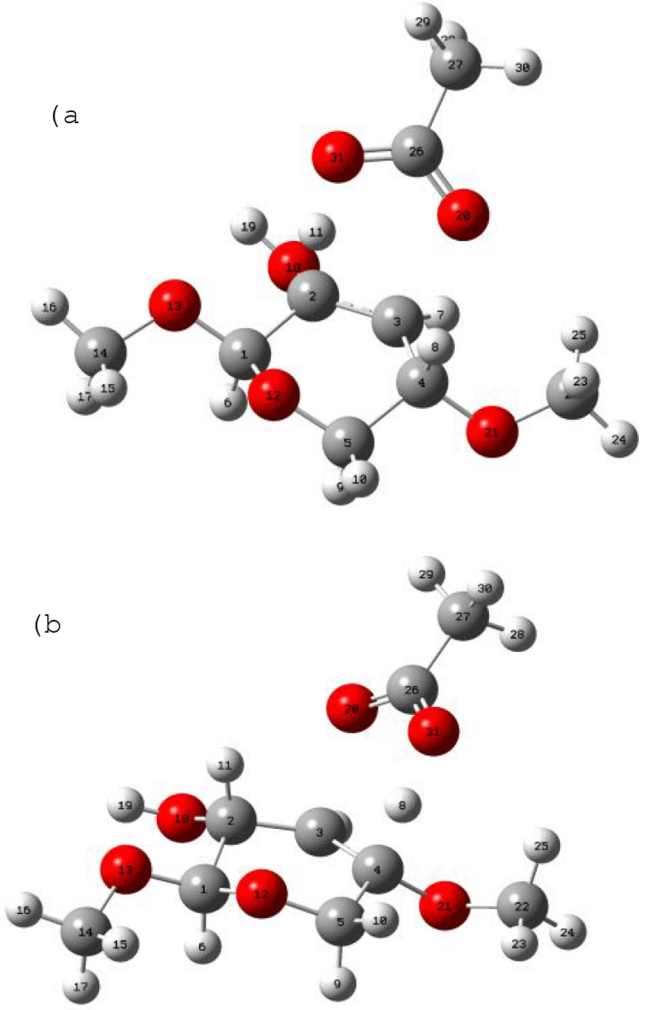

Figure 6. Transition states (TS) structure for the formation of acetic acid from the E-E conformer (d): (a) TS related to reaction (1) and (b) TS related to reaction (2).

barrier heights computed for the E-E conformers are lower than those calculated for the conformer A-A, hydrogen bonds decrease the entropy of the latter more importantly and lead to a higher activation entropy. However, as previously discussed, the transition state related to the A-A conformer remains

https://dx.doi.org/10.1021/acs.energyfuels.0c02901
Energy Fuels XXXX, XXX, XXX−XXX

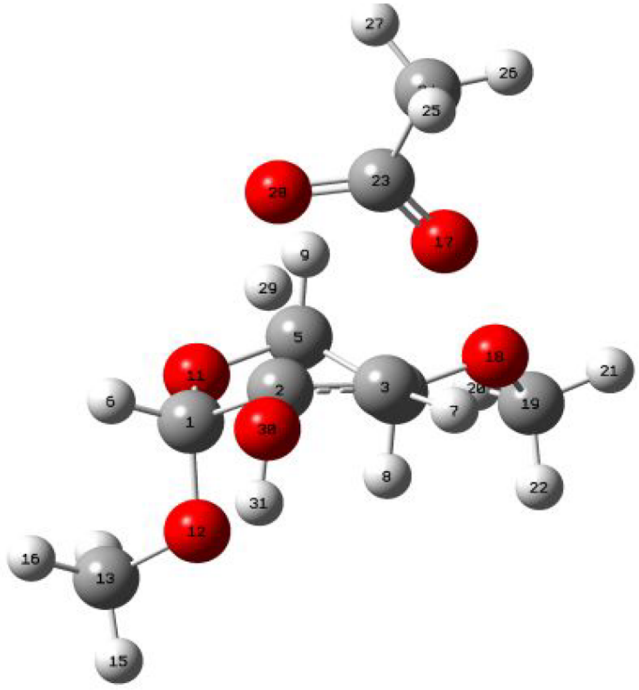

Figure 7. Transition state structure for the formation of acetic acid from the A-A isomer.

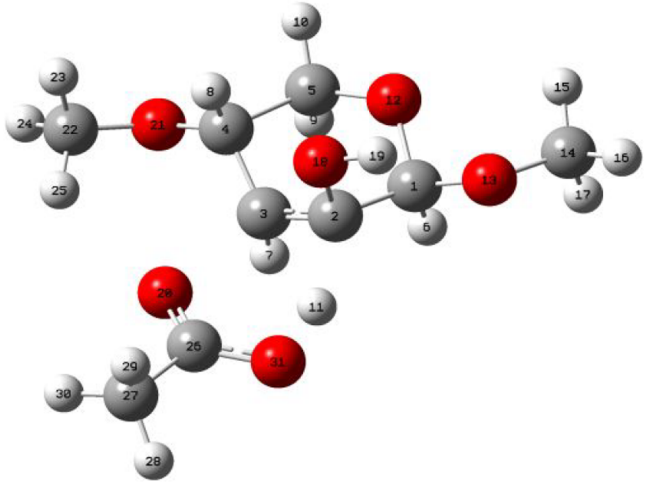

Figure 8. Transition state structure for the formation of acetic acid from the E-A isomer (reaction 1 of Figure 5).

Table 4. Rate Constants for the Formation of Acetic Acid at T = 800 K

	A (s^{-1})	n	E_a (kcal/mol)	k (800 K; s^{-1})
A-A	1.67×10^{13}	0.374	55.67	2.5×10^{-1}
E-A(1)	9.90×10^{12}	0.107	69.19	2.5×10^{-6}
E-A(2)	2.24×10^{13}	0.106	56.00	2.3×10^{-2}
E-E(1)	1.04×10^{9}	1.015	48.48	5.2×10^{-2}
E-E(2)	1.23×10^{10}	0.74	51.52	1.4×10^{-2}

questionable and the transition states occurring during the reaction of the E-E and E-A conformers are more likely to exist. In the following we will no longer consider the A-A conformer. In addition, the magnitude of the activation energy computed for the reaction of the conformer E-A(1) prevents any role of the latter in the formation of acetic acid (Figure 9).

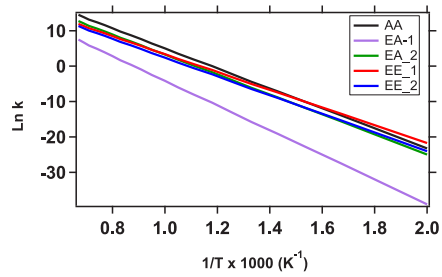

Figure 9. Rate constant (k) as a function of temperature for the formation of acetic acid from the C6-acetyl group.

Until now, it has been shown that the 3-O-acetyl group can result easily in acetic acid by "attracting" the hydrogen atom linked to the C2 position to form the carboxyl group (reaction 2, Figure 5) rather than stabilizing macromolecular radicals; thus preventing polymerization. However, we are also interested in potential "secondary" and low energy molecular reactions subsequent to reactions (1) and (2) (Figure 5). A possible elementary process is the retro Diels–Alder reaction leading to the ring opening of the products according to reactions (3) and (4) (Figure 10).

The calculated energy barriers (Table 5) computed, both at the B3LYP and CBS-QB3 levels of theory are significantly lower than those obtained previously for the formation of acetic acid.

In addition, the reaction rate coefficients obtained at the CBS-QB3 level are given in Table 6 and displayed as a function of temperature in Figure 11.

In Figure 11, we added the rate of formation of acetic acid from the conformer E-E(1) for comparative purpose. These results clearly show that reactions (3) and (4) are preferred over those involving the formation of acetic acid. At T = 800 K, the rate constants of reactions (3) and (4) are respectively 100 and 1500 times faster than the formation of acetic acid from the E-E(1) conformer (Figure 11). If the barrier heights of the retro Diels–Alder are lower, entropic effects are also favored since no internal rotation is hindered during the formation of the transition state. Thus, it can be concluded that the retro-Diels–Alder reaction is not a limiting step and that the products formed during reactions (1) and (2) will be easily decomposed through pathways (3) and (4).

Reaction (4) (Figure 10) leads to the formation of methyl formate (CH_3OCHO) due to the chosen model molecule representative of the C6+acetyl subunit (Figure 1). However, the same C6+acetyl group is connected to another β-D-xylose unit, and the actual structure for the reaction (4) is now shown in Figure 12. Indeed, the probability of finding a new acetyl group on the cyclic structure remains low.

To study the formation of acetic acid and avoid prohibitive time calculations, only the framed part (Figure 12) was kept and a methyl group was added after the oxygen atom. In addition, only one hydroxyl group has been kept in the model molecule because of the critical influence of hydrogen bonding on mechanistic events. The new model molecule, the 4-dihydroxy-6-methoxytetrahydro-2H-pyran-3-yl formate, can undergo pericyclic reactions to form formic acid (Figure 13).

Two reactions can be considered depending on the H atom (reactions (5) and (6) of Figure 13). Since the B3LYP energies were not sufficiently accurate as previously discussed, only the CBS-QB3 barrier heights are given in Table 7.

https://dx.doi.org/10.1021/acs.energyfuels.0c02901
Energy Fuels XXXX, XXX, XXX–XXX

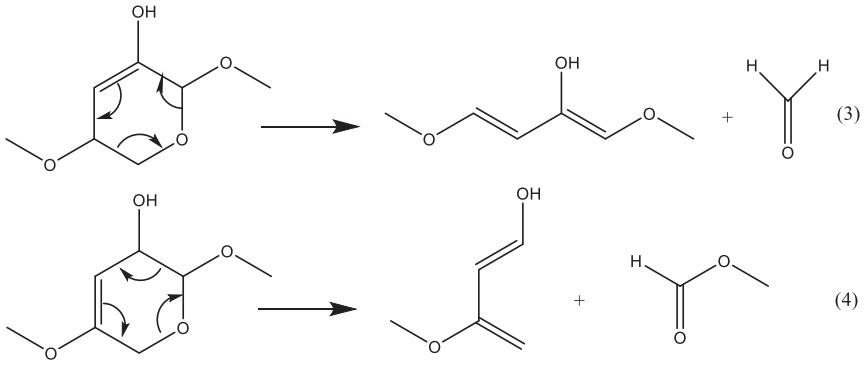

Figure 10. Retro-Diels–Alder reactions involved in the unimolecular decomposition of the products formed in reactions (1) and (2) of Figure 4.

Table 5. Zero-Point Including Energies at 0 K for the Retro Diels-Alder Reactions of Figure 8

E_a (kcal mol^{-1})	reaction (3)	reaction (4)
B3LYP	41.13	37.33
CBS-QB3	47.12	42.24

Table 6. Reaction Rate Coefficients for the Retro Diels-Alder Reaction of Figure 10 and Value of the Rate Constant at T = 800 K, at the CBS-QB3 Level of Theory

	A (s^{-1})	n	E_a(kcal/mol)	k (800 K; s^{-1})
reac (3)	8.51 × 10^{12}	0.432	49.13	5.8
reac (4)	5.74 × 10^{11}	0.639	42.85	80.8

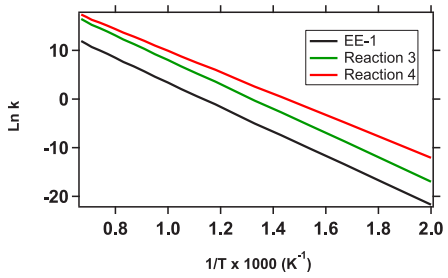

Figure 11. Rate constant (k) as a function of temperature (500–1500 K) for the retro Diels–Alder reactions (Figure 10).

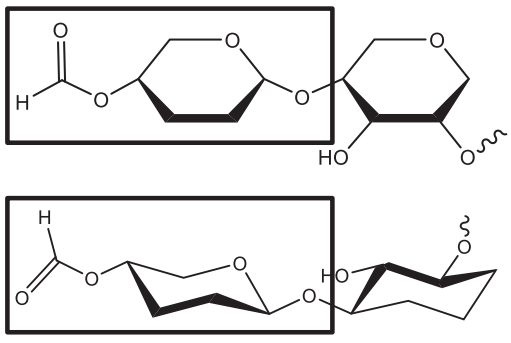

Figure 12. Structure of one of the hemicellulosic fragments of Figure 1 after reactions (3) and (4).

These energy barriers are similar to those obtained for the formation of acetic acid (Table 3, isomer E-E). This result can be explained by the surplus of energy required for the removal of the primary hydrogen compared to that of the secondary hydrogen. Table 8 and Figure 14 display respectively both reaction rate coefficients and the Arrhenius plot.

The formation of formic acid remains slower than the retro Diels–Alder reaction but faster than the formation of acetic acid, thus confirming the trends displayed in Figure 11, where the second pathway involving the formation of acetic acid from E-E(1) was also found as rate-limiting step compared to the corresponding retro Diels–Alder reaction and formic acid formation.

It is worth noting that the repetition of this "secondary" 6-center pericyclic reaction could occur and be a function of the number of xylan units, which represent the backbone of the hemicelluloses. The presence of an initial acetyl group permits to initiate the reaction and then to produce a succession of pericyclic reactions to form formic acid, via reaction (6) and retro Diels–Alder mechanism. Although formic acid has not been detected within the fast pyrolysis condensates (Table S2), either among the primary condensables produced from the fast pyrolysis of all isolated hemicelluloses (Table S3), a number of studies have reported its formation.[39,40] These differences between acids production have been attributed to the variations in heat energy supply to break down the covalent bonds.[8] In the context of this theoretical study, the simulation of the covalent bond breakdown was made by the mechanical stretching of a molecule which is simulated by relaxed potential energy surface scans.[41] The variations linked to energy density differences were not investigated. However, the successive and secondary mechanism proposed (Figure 13) could explain the substantial amount of formic acid.

4.3.2. C5 + Ester Group. The formation of carboxylic acid from concerted reactions has been also performed on α-1,3-L-arabinose in Figure 1 (C5+ester group). To reduce the computational time, a model molecule, depicted in Figure 15, has been considered. In this surrogate, the xylose structure and the methoxyphenol have been replaced by a methyl group. This structure contains 16 heavy atoms and reaches the limit size for CBS-QB3 calculations.

Several scans around the single bonds were considered at the B3LYP/6-31+G(d,p) level of theory in order to find the lower energy conformer. In fact, the energy of each new structure found by scanning was systematically computed at the CBS-QB3 level of theory to ensure that it corresponds to the lower energy conformer, as discussed in section 3. Contrary to the C6+acetyl group, the position of the substituents (axial or equatorial) are fixed to correspond to the spatial arrangement of the α-L-arabinofuranose configuration.[10] As shown in Figure 16, the conformer found favors intramolecular hydrogen bonding interactions with hydroxyl groups minimizing its energy. From this structure, we investigated possible carboxylic acid formation from concerted reactions. Due to the presence

https://dx.doi.org/10.1021/acs.energyfuels.0c02901
Energy Fuels XXXX, XXX, XXX–XXX

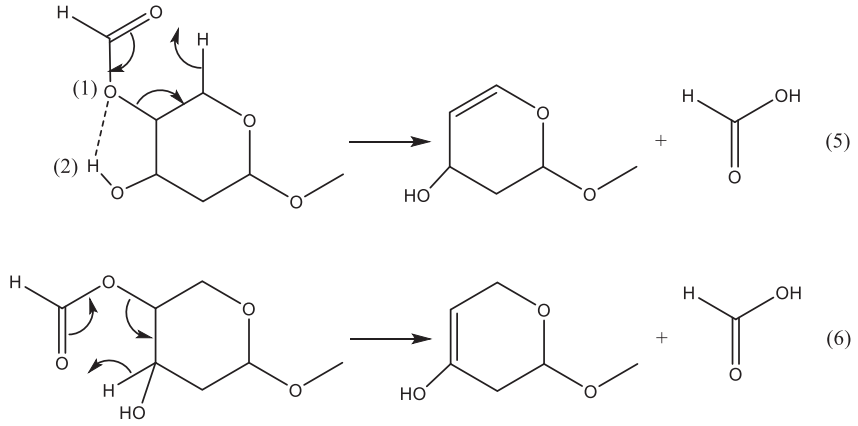

Figure 13. Formation of formic acid through pericylic rearrangements of the 6-methoxytetrahydro-2H-pyran-2-yl formate.

Table 7. Zero-Point Including Energies at 0 K, for the Formation of Formic Acid (Figure 10)

E_a (kcal mol^{-1})	reaction (5)	reaction (6)
CBS-QB3	50.19	50.96

Table 8. Reaction Rate Coefficients of Retro Diels-Alder Reactions (Figure 13) at T = 800 K

	A (s^{-1})	n	E_a (kcal/mol)	k (800 K; s^{-1})
reac (5)	2.21 × 10^{12}	0.646	50.34	2.9
Reac (6)	1.42 × 10^{14}	0.047	53.62	4.4× 10^{-1}

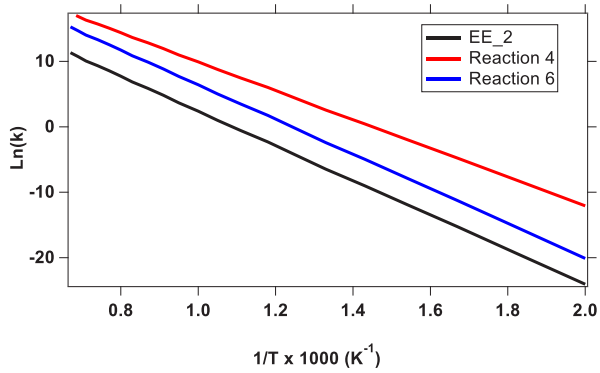

Figure 14. Comparison between rate constants (k) as a function of temperature for the formation of acetic acid from the conformer E-E(2), for the retro Diels–Alder reaction (reaction 4, Figure 10) and for the formation of formic acid (reaction 6, Figure 11).

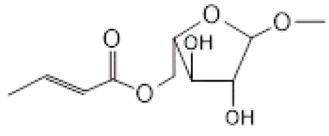

Figure 15. Structure considered in the study of the C5+ester group.

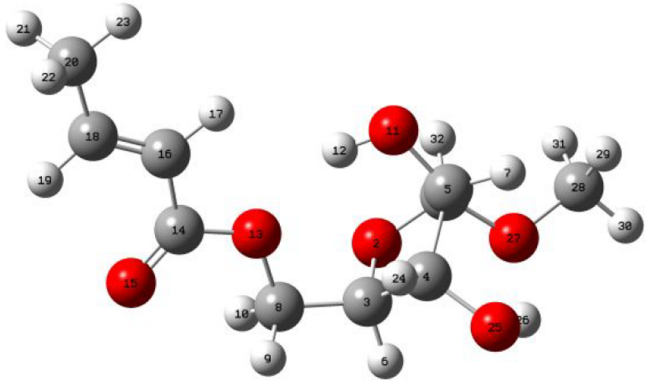

Figure 16. Lower energy conformer found, at the CBS-QB3 level of theory, for the C5+ester presented in Figure 12.

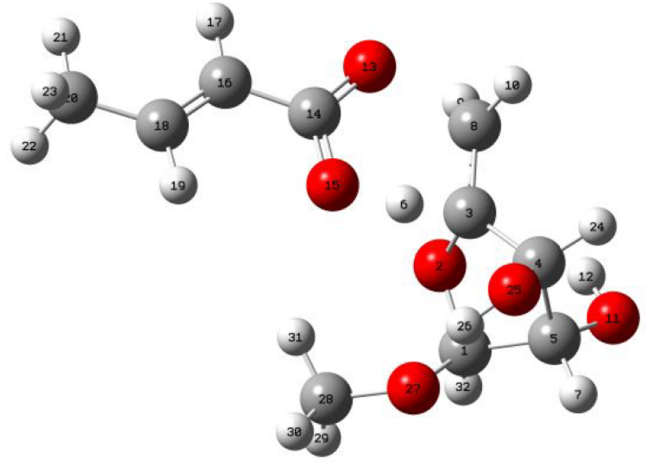

Figure 17. Six-membered transition state (TS) obtained at the CBS-QB3 level of theory for the formation of carboxylic acid from the C5+ester group.

of an ester function, it is possible to transfer the hydrogen atom H6 (Figure 16) from the carbon C3 to the oxygen O15 via a 6-membered ring transition state (Figure 17). The model molecule used leads to the formation of 2-butenoic acid, which corresponds to the ferulic acid considering the whole subunit, α-1,3-L-arabinose with ferulic acid (Figure 1).

The energy barrier computed at the CBS-QB3 level is equal to 50.78 kcal/mol. It is worth noting that the value obtained, at the CBS-QB3 level of theory is close to those obtained for the formation of acetic acid from the C6+acetyl subunit (conformer E-E of Table 3). Despite slight variations in the molecular environment, the nature of the transferred hydrogen atom, which is a tertiary hydrogen atom, remains the same.

Another possible concerted reaction involving the formation of ferulic acid from the C5+ester group, implies a 4-membered ring (Figure 18).

Indeed, the H6 atom previously transferred to the O15 oxygen atom of the ester function can now be transferred to

https://dx.doi.org/10.1021/acs.energyfuels.0c02901
Energy Fuels XXXX, XXX, XXX−XXX

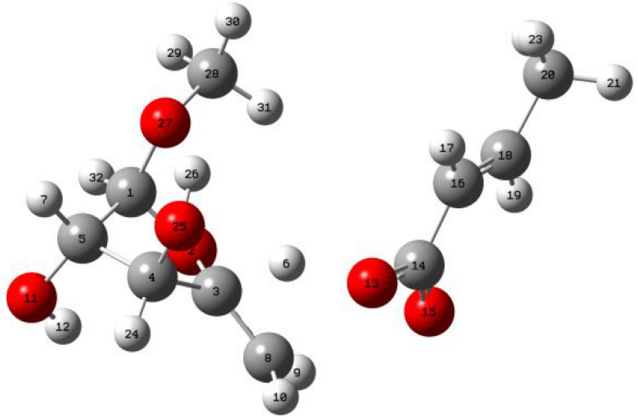

Figure 18. Four-membered TS Lower energy conformer found, at the CBS-QB3 level of theory, for the C5+ester presented in Figure 13.

the O13, while the C−O bond is broken (C8_O13). The barrier height calculated is equal to 68.28 kcal/mol at 0 K, which is notably greater than that of the previous concerted reaction. This is mainly due to the higher ring strain energy of the transition state. Reaction rate coefficients have been calculated and are presented in Table 9.

Table 9. Rate Constants for the Formation of Ferulic Acid (Figures 17 and 18) at T = 800 K

	A (s^{-1})	n	E_a (kcal/mol)	k (800 K; s^{-1})
6-membered ring	4.67×10^{10}	1.148	48.05	7.5
4-membered ring	1.17×10^{11}	1.236	66.17	3.8×10^{-4}

As mentioned previously, the carboxylic acid formed from the concerted reaction is the ferulic acid. However, no ferulic acid has been observed experimentally suggesting that it is readily transformed via molecular or radical reactions. A thermogravimetric analysis performed by Fiddler et al.,[12] investigating the pyrolysis of ferulic acid, has showed that unsubstituted and substituted guaiacols (i.e., 4-methyl, 4-ethyl, and 4-vinylguaiacol) were released as main primary products. Guaiacol and 4-vinylguaiacol have been observed experimentally in this study (Tables S2 and S3), and we therefore investigated their formation. Figure 19 shows the TS occurring during the formation of vinyl-guaiacol and CO_2 based on a concerted reaction involving a H transfer from the acid group to the vinylic carbon atom.

The energy barrier computed at the CBS-QB3 level of theory is equal to 63.7 kcal/mol: a value rather high due to the constrained transition state structure (4-membered ring). In this context, it is reasonable to assume that radical reactions could also have a role in the formation of 4-vinyl-guaiacol from ferulic acid. Indeed, a possible radical pathway involves the H-abstraction of the acid function, followed by a β-scission leading to CO_2 and a free radical. This latter species can react in turn by H-abstraction to form the 4-vinyl-guaiacol. Since this study only focuses on molecular reactions, we did not investigate this radical pathway. Another possible molecular reaction is the formation of guaiacol from a 4-centered transition state, showen in Figure 20. In this concerted reaction, the hydrogen (H4) atom located on the vinylic carbon atom (C2) is transferred to the carbon (C9) located on the aromatic cycle, while the C1−C9 bond is broken.

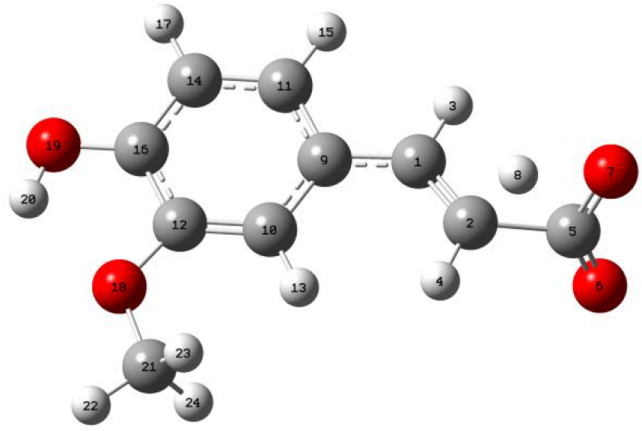

Figure 19. Transition state structure for the formation of 4-vinyl-guaiacol from ferulic acid.

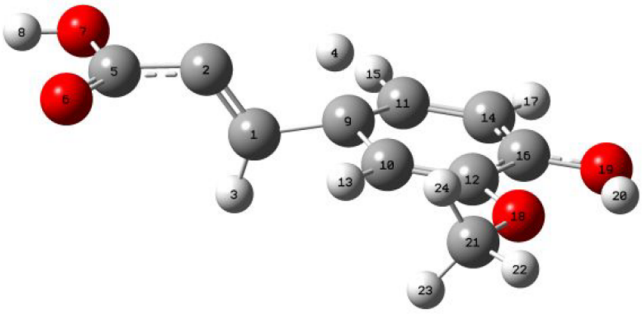

Figure 20. Transition state structure for the formation of guaiacol from ferulic acid.

It is worth noting that no transition state has been located on the potential energy surface, at the level of theory used in CBS-QB3 (i.e., B3LYP/6-311G(d,p)). However, an optimized structure has been identified at the M062X/6-311+G(d,p) level. From the optimized geometry, an energy calculation identical to that used in CBS-QB3 has been performed to deduce the energy barrier. For the sake of consistency, the same procedure has been used for the reactant. However, the H transfer from the vinyl group displays a high energy barrier of 98.89 kcal/mol, which makes this reaction kinetically insignificant. The last concerted reaction envisaged is a 6-membered ring TS and consists of the acidic H atom transfer to the aromatic carbon, leading to the formation of CO_2, acetylene, and guaiacol (Figure 21).

To reach this transition state, the ferulic acid must have a cis configuration to avoid an internal rotation around the π bond of the vinylic structure. The high computed energy barrier of 77.62 kcal/mol indicates that this concerted reaction is unlikely to happen and therefore explain the formation of guaiacol or vinyl-guaiacol. In this case, radical reactions can compete with the molecular ones. Radical mechanisms for ferulic acid (FA) decomposition have been proposed by Verma et al.[42] FA was converted into vinyl-guaiacol after decarboxylation, which in turn could be either way be transformed into eugenol/*cis*-isoeugenol/4-ethylguaiacol and vanillin/acetovanillone through a methyl group addition or a hydroxyl migration, respectively.

4.3.3. C6 + Carboxylic Group. The glucuronic acid substituents are one of the typical branching motifs of heteroxylans in grass.[10] The "C6 + carboxylic group" system

https://dx.doi.org/10.1021/acs.energyfuels.0c02901
Energy Fuels XXXX, XXX, XXX−XXX

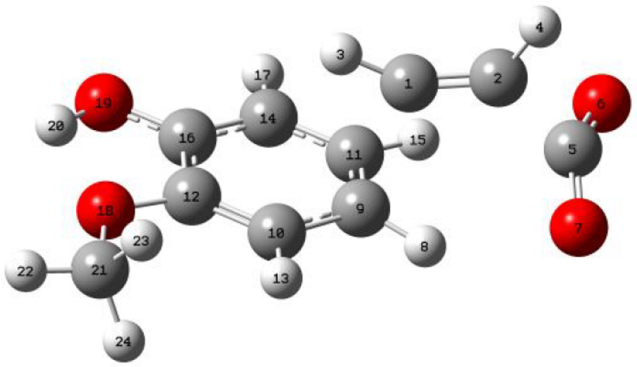

Figure 21. Transition state structure for the formation of guaiacol from ferulic acid through a 6-membered ring TS.

is a combination of a xylose unit combined with a carboxylic group attached to xylose (Figure 1). Following the approach used for the previous fragments, methyl groups were used to replace the saccharide units to reduce computational costs and the equatorial positions of the CH_3−O groups were "frozen". Figure 22 presents the eight possible configurations for this system that result from the combination of all possible axial/equatorial orientations of the two hydroxyl and carboxylic groups.

For each configuration presented in Figure 22, the lowest energy conformer was identified by using successive relaxed scans (B3LYP/6-31+G(d,p)) of the internal rotations of the OH and carboxylic groups. CBS-QB3 calculations were performed on the lowest energy conformers identified, and the results are displayed in Table 10.

Table 10. Relative Difference between Energies at 0 K of the Eight Configurations for the "C6+Carboxylic" Subunit Relative to the Lowest Energy[a]

E_a (kcal mol^{-1})	B3LYP/6-311G(d,p)	CBS-QB3
(a) A-A-A	1.5	1.1
(b) A-A-E	0.9	0.0
(c) A-E-A	0.0	0.6
(d) A-E-E	0.3	0.2
(e) E-A-A	0.4	0.3
(f) E-A-E	1.1	1.5
(g) E-E-A	1.0	1.9
(h) E-E-E	1.0	1.4

[a]A and E denote axial and equatorial positions as depicted in Figure 22.

DFT and composite methods both predict that the eight configurations are very close in energy (within 2 kcal/mol). The B3LYP computed energies identify the lowest energy conformer as the axial−equatorial−axial configuration, while more accurate CBS-QB3 calculations predict that the axial−axial−equatorial configuration is the lowest energy one. When

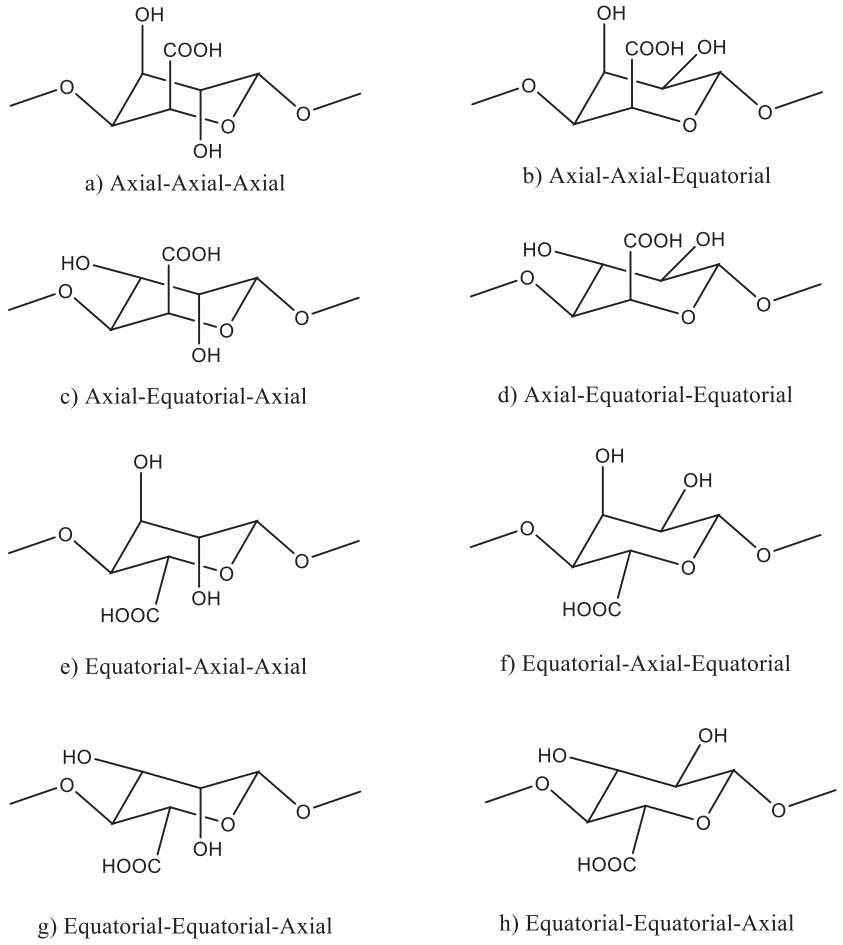

Figure 22. Representation of the eight configurations of the C6 + carboxylic group fragment.

https://dx.doi.org/10.1021/acs.energyfuels.0c02901
Energy Fuels XXXX, XXX, XXX−XXX

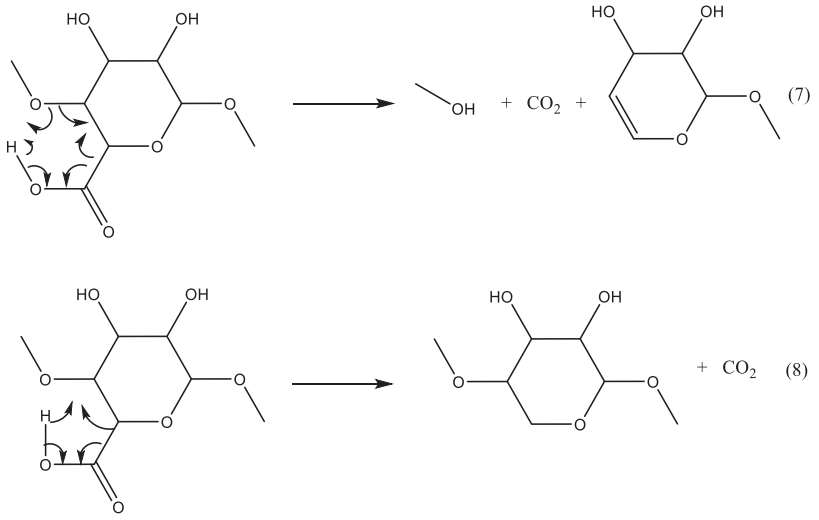

Figure 23. Elementary mechanisms leading to the elimination of CO_2.

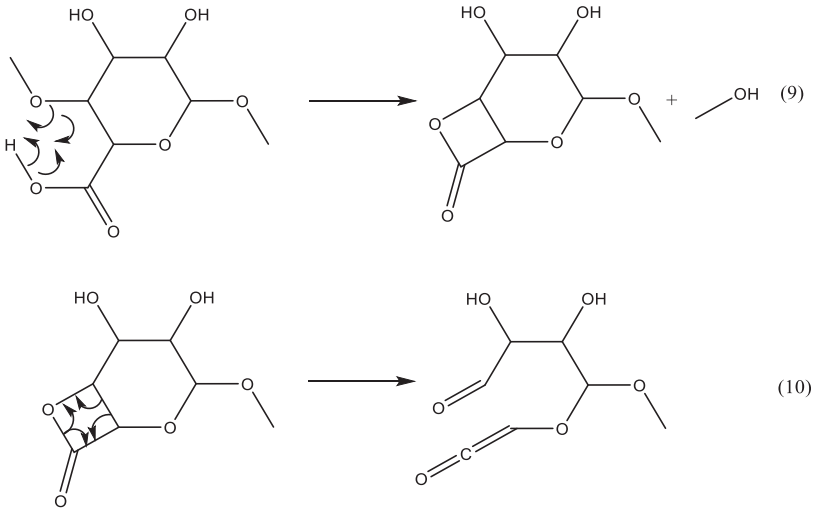

Figure 24. Alternative mechanisms to reaction (7) for equatorial carboxylic group.

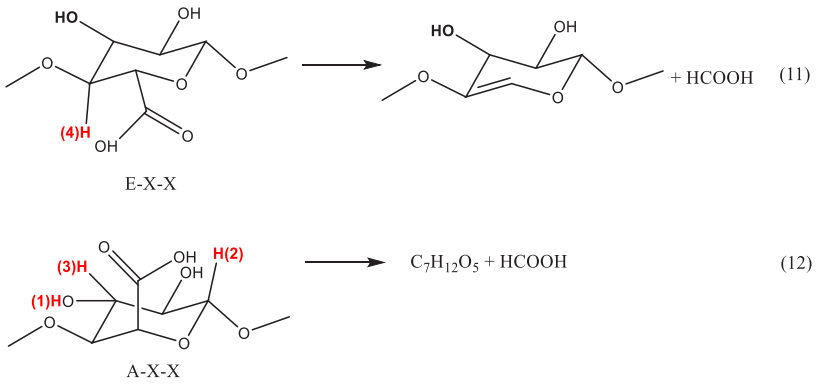

Figure 25. Direct eliminations of formic acid in "C6 + carboxylic" group. Possible H atoms participating to the elementary mechanism are highlighted in red.

the carboxylic group is in an axial orientation, there is a hydrogen bond between the H atom of the acid and the O atom of the glycosylic bond. When the carboxylic group is equatorial, the hydrogen bond involving the acid H atom is different and bound to the O atom in the C6 structure.

For all of the configurations of the "C6 + carboxylic group" fragment, two types of pericyclic elimination were envisaged: CO_2-eliminations and HCOOH-eliminations. Each of the CO_2-elimination reactions can occur through different elementary mechanisms (Figures 23 and 24).

https://dx.doi.org/10.1021/acs.energyfuels.0c02901
Energy Fuels XXXX, XXX, XXX−XXX

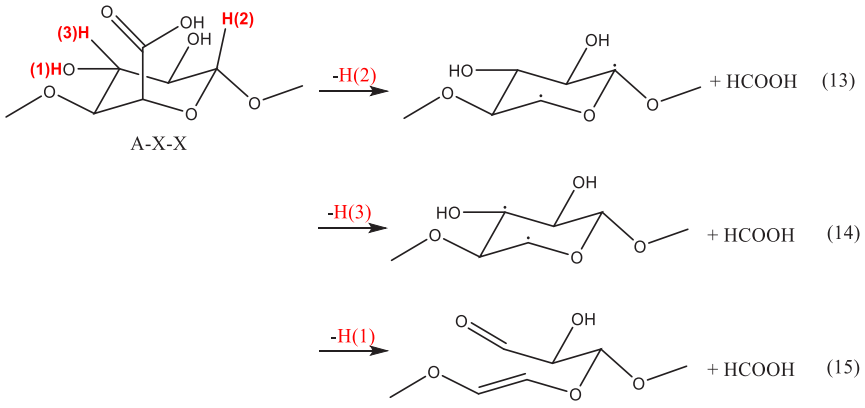

Figure 26. Products of the HCOOH-eliminations in "C6 + carboxylic" structures with axial orientation of the COOH group.

CO_2-eliminations were systematically explored for all of the configurations presented in Figure 22. Reaction (8) suggests the transfer of the H atom of the carboxylic acid group to the carbon atom bearing it, while the C−C(OOH) bond is broken. Reaction (7) is a 6-center pericyclic reaction. Theoretical calculations showed that the direct elimination of CO_2 (reaction (7)) is possible only for configurations where the carboxylic acid group is in axial position. When it is in the equatorial position, the left-hand side of reaction (7) leads to a bicyclic structure (Figure 24).

An examination of the transition state structures of reaction (9) of E-X-X configurations show that the formation of a nascent π bond (as in reaction (7)) would require an inversion of the chair conformation of the cyclic part of the molecule. Therefore, the most favored pathways lead to the formation of the bicyclic structure. IRC calculations performed at the B3LYP/6-31+G(d,p) level of theory confirmed this mechanism. The fate of the bicyclic structure formed in reaction (9) that still requires the breaking of a glycosylic bond is presented in reaction (10). A 4-center rearrangement would facilitate the opening of the C6 unit.

The elimination mechanisms of formic acid were also investigated (Figure 25).

The complexity of the HCOOH-eliminations depends on the orientation of the carboxylic group. If the COOH group is in the equatorial position (configurations e−h), the only internally abstractable H atom is in γ-position of the carboxylic group (reaction (11) in Figure 25). This reaction yields formic acid and an unsaturated C6 cycle that keeps the initial orientation of the two hydroxyl groups. The number of possible H atom that can be internally abstracted in the HCOOH-elimination is greater when the carboxylic group is in the axial position. In Figure 26, it can be seen that three different H atoms (H(1−3)) can participate in the elementary HCOOH-elimination mechanism. For all of the configurations featuring an axial COOH group (structures a−d in Figure 22), the hydrogen atom H(2) can be involved. The internal transfer of H atoms H(3) and H(1) in Figure 26, yielding $C_7H_{12}O_5$ and HCOOH depends on the orientation of the OH group in β-position of the glycosylic bond. If it is in the axial position, then the OH and COOH groups are facing each other and H1 can be transferred. Otherwise, H(3) can be abstracted by the COOH group.

The transfer of H atoms H(2) and H(3) yields zwitterionic structures that were found to be true minima on the potential energy surface (B3LYP/6-311G(d,p) geometry optimizations). The HCOOH-elimination involving H(1) (reaction (15)) leads to the opening of the cyclic structure, but without the breaking of the glycosylic bonds.

The computed energy barriers (Table 11) show that the direct CO_2 elimination (reaction (7)) from configurations with the carboxylic group in axial orientation is the most favored. If this group is in an equatorial orientation, the equivalent reaction leads to the formation of a bicyclic structure (reaction (9)).

Table 11. Energy Barriers (CBS-QB3) at 0 K of CO_2-Eliminations (Reactions (7) to (10)) for All Configurations of the "C6 + Carboxylic Acid" Fragment

	CO_2-eliminations			
reaction no.	(7)	(8)[a]	(9)	(10)
(a) A-A-A	55.9	73.9[c]		
(b) A-A-E	57.2	76.5[c]		
(c) A-E-A	53.3	76.8[b]		
(d) A-E-E	54.3	74.2[c]		
(e) E-A-A		71.5[b]	72.4	37.4
(f) E-A-E		71.7[b]	69.8	42.5
(g) E-E-A		71.1[b]	72.0	44.5
(h) E-E-E	-	70.9[b]	71.9	44.3

[a]Lowest energy conformation. H atom transfer from COOH group can occur in "cis" or "trans" conformations. [b]"cis" OH from COOH 'eclipsed' with the H atom linked to the carbon bearing the COOH group. [c]"trans" =O from COOH eclipsed with the H atom linked to the carbon bearing COOH.

CBS-QB3 calculations show that the energy barrier associated with this reaction leads to critical energies lying about 20 kcal/mol above the energy barriers of reaction (7). The ring opening reaction of the bicyclic structure (reaction (10)) is found to occur with relatively low activation energies, but the kinetic limiting step is the formation of the bicyclic structure (reaction (9)).

The alternative direct CO_2-elimination, occurring through a 4-center transition state structure (reaction (8)), is predicted to be in the range of 71−77 kcal/mol. Lower energy barriers are computed for an equatorial orientation of the carboxylic acid group compared to configurations with an axial orientation. In the latter case, reaction (7) will always be favored over reaction (8). For an equatorial orientation, the reactions (8) and (9) are in competition.

The variations in energy barriers observed for a given orientation of the COOH group (axial or equatorial) reflect

https://dx.doi.org/10.1021/acs.energyfuels.0c02901
Energy Fuels XXXX, XXX, XXX−XXX

the complex variations in hydrogen bonding in the "C6 + carboxylic acid" reactant and the transition state geometries of each elementary reactions. The hydrogen bonds may form between the H atoms of the hydroxyl groups and, depending on the configuration studied, the oxygen atoms of the cycle, of the glycosylic bonds and of the OH groups themselves.

Energy barriers, computed at the CBS-QB3 level of theory, for HCOOH-eliminations are given in Table 12.

Table 12. Energy Barriers (CBS-QB3) at 0 K of HCOOH-Eliminations (Reactions (11) and (13) to (15))

	HCOOH-eliminations			
reaction no.	(11)	(13)	(14)	(15)
(a) A-A-A		78.0		76.1
(b) A-A-E		82.7		82.4
(c) A-E-A		79.7	95.5	
(d) A-E-E		81.4	84.2	
(e) E-A-A	93.2			
(f) E-A-E	91.3			
(g) E-E-A	90.9			
(h) E-E-E	85.9			

For an equatorial orientation of the carboxylic acid group, only reaction (11) is possible with computed energy barriers ranging between 85.9 and 93.2 kcal/mol. These barriers are too high to compete with CO_2-elimination reactions (8) and (9). The same conclusion can be reached for an axial orientation of the carboxylic group where the calculated activation energies of reactions (13) to (15) lie at least 22 kcal/mol above the computed critical energies of reaction (7). Therefore, the direct formation of HCOOH from the "C6 + carboxylic acid" group is unlikely to occur compared to the other possible decomposition pathways of this fragment, which contradicts some previous proposed mechanisms for the formic acid formation.[9]

Since the energy barriers of direct CO_2-eliminations (reaction (7)) lie at least 15 kcal/mol below the critical energies of other decomposition routes, rate constants were computed only for these mechanisms (Figure 27).

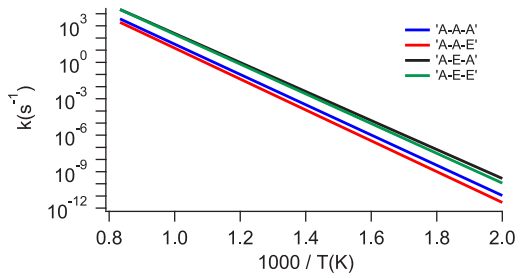

Figure 27. High-pressure rate constants of direct CO_2 elimination (reaction (7)).

It can be seen in Figure 27 that the rate constants for reaction (7) are higher by a factor of ~10 when the OH group located in β-position of the C atom linked to the glycosylic bond is in an equatorial position. At 700 K, the rate constant for the direct CO_2-elimination of A-E-A is 1.81×10^{-3} s^{-1}.

The fate of the fragment produced in reaction (7) was also investigated using theoretical calculations. Figure 28 depicts the reaction mechanism considered in our calculations.

In reaction (16) a retro-Diels–Alder decomposition leads to the release of 3-hydroxyprop-2-enal. Four different configurations can decompose through reaction (7), yielding four different configurations depending on the reactant structure of reaction (16) and the orientations of its OH groups: A-A, A-E, E-A, and E-E. Relative energies of the different configurations of the unsaturated 6-membered ring in reaction (16) are given in Table 13.

Table 13. Relative Energies at 0 K of the Four Configurations of the Reactant Molecule of Reaction (16), Relative to the Lowest Energy[a]

E (kcal mol^{-1})	B3LYP/6-311G(d,p)	CBS-QB3
(a) A-A	0.5	0.4
(b) A-E	0.2	1.4
(c) E-A	0.1	0.5
(d) E-E	0.0	0.0

[a]A and E denote axial and equatorial positions of OH–groups as depicted in Figure 22.

B3LYP/6-311G(d,p) and CBS-QB3-based computations predict that the equatorial-equatorial orientation of the OH groups is the lowest energy configuration. All configurations lie in a small range of energy. All rate constants were therefore determined (Table 14).

Table 14. High-Pressure Limit Rate Constants (k_∞) Computed at the CBS-QB3 Level of Calculation for Retro-Diels-Alder Reaction (16): $k_\infty = AT^n \exp(-E_a/RT)$

	A (s^{-1})	n	E_a (kcal/mol)
(a) A-A	1.37×10^9	1.488	45.6
(b) A-E	1.07×10^{13}	0.506	46.0
(c) E-A	1.48×10^{11}	0.731	44.6
(d) E-E	3.25×10^{10}	1.036	45.1

For all of the configurations, the activation energy of reaction (16) is around 45 kcal/mol. Therefore, in the subsequent decomposition of the sugar acid fragment through reaction (7), followed by reaction (16), the initial decomposition (7) is the limiting step with an energy barrier of about 55 kcal/mol.

The lowest energy overall decomposition route of this fragment yields 3-hydroxyprop-2-enal, the same byproducts that can lead to further small oxygenates (Figure 29).

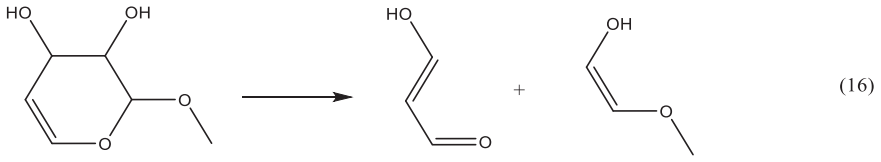

Figure 28. Elementary mechanisms for the decomposition of the fragment product of reaction (7).

https://dx.doi.org/10.1021/acs.energyfuels.0c02901
Energy Fuels XXXX, XXX, XXX–XXX

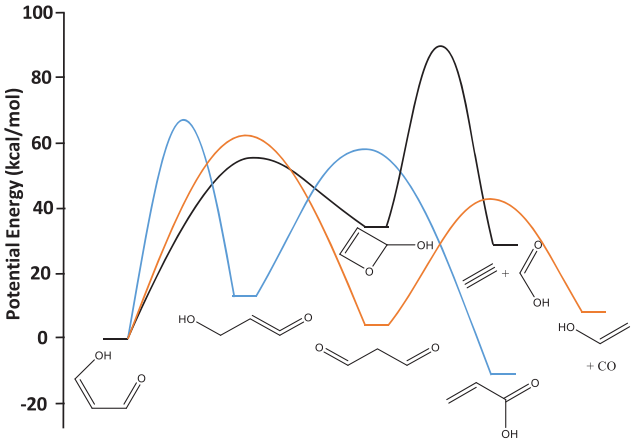

Figure 29. Potential energy surface of 3-hydroxyprop-2-enal unimolecular decomposition (CBS-QB3 computations).

Three different unimolecular decomposition routes can occur. The lowest energy barrier for the initial decomposition step of 3-hydroxyprop-2-enal leads to the formation of the cyclic 2H-oxet-2-ol. However, according to the quasi-steady state approximation described by Laidler,[43] its decomposition into formic acid and acetylene faces a high energy barrier (89.9 kcal/mol relative to 3-hydroxyprop-2-enal, black line in Figure 29). The two most favored decomposition pathways for 3-hydroxyprop-2-enal conversion involve (i) the formation of 3-hydroxyprop-1-en1-one that can rearrange into prop-2-enoic acid (blue line in Figure 29) and (ii) the formation of propendial that further decomposes into ethenol and CO (orange line in Figure 29). From the potential energy surface, the formation of ethenol and CO is favored over the formation of prop-2-enoic acid, with a limiting energy barrier of 63.3 kcal/mol vs 66.9 kcal/mol. Based on computed rate constant calculations of the elementary steps, we performed a quasi steady state approximation (QSSA) on the ketene and dial intermediates to determine the rate constant of 3-hydroxyprop-2-enal conversion. The calculated QSSA rate constant for 3-hydroxyprop-2-enal to prop-2-enoic acid is $k_\infty = 3.91 \times 10^{09} T^{1.086} \exp(-65503/RT)$ and is $k_\infty = 4.30 \times 10^{06} T^{2.284} \exp(-59240/RT)$ for 3-hydroxyprop-2-enal to ethenol + CO (units are s^{-1} and cal/mol). The computed rate constants show that, from 500 to 1000 K, the branching ratios to ethenol + CO are greater than 99%.

To summarize, the unimolecular elimination reaction of the fragment "C6+carboxylic acid" first leads to the elimination of CO_2 through reaction (7). This process breaks down the polymer chain of xylose units with the two O atoms of the glycosylic bonds transformed into a hydroxyl group and a 2,4-dihydro-2H-pyran-3,4-diol group. The latter group decomposes through a retro-Diels–Alder mechanism (reaction (16)) and yields 3-hydroxyprop-2-enal that ultimately decomposes into ethenol and CO. In turn, ethenol could yield formaldehyde, with an energy barrier of 57.1 kcal/mol (CBS-QB3 level of theory). The branching ratios of the products of the "C6+glucuronic" decomposition are computed here in the gas phase, but the formation of prop-2-enoic acid could also be favored through catalytic mechanisms that remain to be identified.

5. CONCLUSION

The primary goal of this investigation was to reveal some potential mechanisms leading to the formation of small oxygenates from the pyrolysis of an hemicellulosic fragment. The use of molecular probes has permitted to confirm the different building blocks of hemicelluloses and structural changes induced by extraction and purification techniques. This molecular technique has been proven to be complementary to conventional sugar analyses. Those structural changes have been related to the chemical composition of volatiles released during fast pyrolysis. This comparison has confirmed the critical role of alkali-based pretreatments of biomass on the chemical composition of pyrolysis volatiles.

Modeling results that mainly focused on oxygenates formation pathways have revealed a few key thermodynamic and chemical features. The modeled thermal decomposition of the C6 + acetyl group (subunit of the glucuronoarabinoxylanan studied) in the gas phase (under the reaction-controlled conditions) was initiated with a concerted pathway, a pericyclic reaction to form acetic acid and a pyran compound, a mechanism strongly influenced by the stabilizing effect of hydrogen bonding. The same primary pathway could be followed by a secondary retro Diels–Alder reaction releasing lighter oxygenates. It has been demonstrated that temperature affects the stability of conformers changing the course of reactional rearrangement and rates: at lower temperature (650 K) hydrogen bonding is more prevalent and the formation of acetic acid even faster in the case of pericyclic reaction. At higher temperature (800 K), the formation of formic acid through a succession of pericyclic reactions is preferred, and its yield influenced by the repetition of β-D-xylose units.

The mechanistic study made on the "C5 + ester group" subunit indicated that its conversion led to the formation of 4-vinylguaiacol, usually attributed to the transformation of lignins, through concerted or radical mechanisms. The calculations revealed a potential competition between those two nonionic reactions. Finally, the transformation of the "C6 + glucuronic acid" has been found to be highly sensitive to the type of conformations. Variations in axial and equatorial positions of hydroxyl and carboxylic groups greatly affect hydrogen bonding and therefore the course of conversion. The unimolecular elimination reactions proposed have not been able to confirm the formation of formic acid.

Overall, our investigation suggests a degradation network for the conversion of a typical hemicellulosic fragment found in grassy biomass into small oxygenates. Concerted mechanisms have been clearly showed to be in competition with radical mechanisms and the corresponding intrinsic kinetic data sets were determined.

■ ASSOCIATED CONTENT

Supporting Information

The Supporting Information is available free of charge at https://pubs.acs.org/doi/10.1021/acs.energyfuels.0c02901.

S1-Extraction and purification of hemicellulosic samples: Hemi-2 and Hemi-3 with Figure S1: Tangential flow filtration process and Figure S2: Illustrated strategy of hemicelluloses extraction. S2-Colorimetric enzyme-linked immunosorbent assays (ELISAs) with Table S1: List of antibodies used, Table S2: List of condensates obtained from the fast pyrolysis of the isolated hemicelluloses (Hemi-1) identified and quantified by

https://dx.doi.org/10.1021/acs.energyfuels.0c02901
Energy Fuels XXXX, XXX, XXX–XXX

GC/MS, Table S3: List of condensable compounds detected and identified by Py-GC/MS and the NIST17 databank, and Table S4: Cartesian coordinates of reactants and structures involved in all tables of the article, at the CBS-QB3 level of theory. (PDF)

AUTHOR INFORMATION

Corresponding Author

Marion Carrier − *Energy and Bioproducts Research Institute (EBRI), Aston University, Birmingham B4 7ET, United Kingdom; RAPSODEE, CNRS UMR 5203, Université de Toulouse, IMT Mines Albi, Campus Jarlard, 81013 Albi, France;* orcid.org/0000-0003-4740-3416; Email: marion.carrier@mines-albi.fr

Authors

René Fournet − *Laboratoire Réactions et Génie des Procédés (LRGP), Université de Lorraine, CNRS, 54001 Nancy, France*

Baptiste Sirjean − *Laboratoire Réactions et Génie des Procédés (LRGP), Université de Lorraine, CNRS, 54001 Nancy, France;* orcid.org/0000-0002-8682-5219

Sam Amsbury − *Centre for Plant Sciences, School of Biology, University of Leeds, Leeds LS2 9JT, United Kingdom*

Yoselin Benitez Alfonso − *Centre for Plant Sciences, School of Biology, University of Leeds, Leeds LS2 9JT, United Kingdom*

Pierre-Yves Pontalier − *Laboratoire de Chimie Agro-Industrielle, INPT-ENSIACET, Université de Toulouse, 31030 Toulouse, France*

Anthony Bridgwater − *Energy and Bioproducts Research Institute (EBRI), Aston University, Birmingham B4 7ET, United Kingdom*

Complete contact information is available at: https://pubs.acs.org/10.1021/acs.energyfuels.0c02901

Funding

Action H2020-MSCA-IF-2014, Pyrochem, Grant 656967, entitled "Biopolymers 13C Tracking during Fast Pyrolysis of Biomass - A 2-Level Mechanistic Investigation".

Notes

The authors declare no competing financial interest.

ACKNOWLEDGMENTS

Technical support from Nicolas Beaufils for hemicellulose extraction carried at LCA (Toulouse) and from Joël Rosa for harvesting and providing *Zea mays biomass* grown in natural soils (Gers, France) is warmly acknowledged. The authors also acknowledge the French scientific program MOPGA (reference ANR-18-MPGA-0013) managed by the National Research Agency and financially supported by the "Investissements d'Avenir and "La Région d'Occitanie". High performance computing resources were partially provided by the EXPLOR center hosted by the University of Lorraine. This work was also granted access to the HPC resources of IDRIS under the allocation 2019-A0010807249 made by GENCI.

ABBREVIATIONS

TS, transition state; QSSA, quasi steady state approximation; A, axial; E, equatorial; IRC, intrinsic reaction coordinate

REFERENCES

(1) Vinu, R.; Broadbelt, L. J. Unraveling Reaction Pathways and Specifying Reaction Kinetics for Complex Systems. *Annu. Rev. Chem. Biomol. Eng.* **2012**, *3* (1), 29−54.

(2) Seshadri, V.; Westmoreland, P. R. Concerted Reactions and Mechanism of Glucose Pyrolysis and Implications for Cellulose Kinetics. *J. Phys. Chem. A* **2012**, *116*, 11997−12013.

(3) Vinu, R.; Broadbelt, L. J. A Mechanistic Model of Fast Pyrolysis of Glucose-Based Carbohydrates to Predict Bio-Oil Composition. *Energy Environ. Sci.* **2012**, *5*, 9808−9826.

(4) Ranzi, E.; Eduardo, P.; Debiagi, A.; Frassoldati, A.; Chimica, D.; Chimica, I.; Natta, G.; Milano, P.; Leonardo, P. Mathematical Modeling of Fast Biomass Pyrolysis and Bio-Oil Formation. Note II: Secondary Gas-Phase Reactions and Bio-Oil Formation. *ACS Sustain. Chem. Eng.* **2017**, *5*, 2882−2896.

(5) Ranzi, E.; Cuoci, A.; Faravelli, T.; Frassoldati, A.; Migliavacca, G.; Pierucci, S.; Sommariva, S. Chemical Kinetics of Biomass Pyrolysis. *Energy Fuels* **2008**, *22* (6), 4292−4300.

(6) Ranzi, E.; Debiagi, P. E. A.; Frassoldati, A. Mathematical Modeling of Fast Biomass Pyrolysis and Bio-Oil Formation. Note I: Kinetic Mechanism of Biomass Pyrolysis. *ACS Sustainable Chem. Eng.* **2017**, *5*, 2867−2881.

(7) Dussan, K.; Dooley, S.; Monaghan, R. Integrating Compositional Features in Model Compounds for a Kinetic Mechanism of Hemicellulose Pyrolysis. *Chem. Eng. J.* **2017**, *328*, 943−961.

(8) Carrier, M.; Windt, M.; Ziegler, B.; Appelt, J.; Saake, B.; Meier, D.; Bridgwater, A. Quantitative Insights into the Fast Pyrolysis of Extracted Cellulose, Hemicelluloses, and Lignin. *ChemSusChem* **2017**, *10* (16), 3212−3224.

(9) Patwardhan, P. R.; Brown, R. C.; Shanks, B. H. Product Distribution from the Fast Pyrolysis of Hemicellulose. *ChemSusChem* **2011**, *4* (5), 636−643.

(10) Scheller, H. V.; Ulvskov, P. Hemicelluloses. *Annu. Rev. Plant Biol.* **2010**, *61* (1), 263−289.

(11) Ren, J.; Sun, R. Hemicelluloses. *In Thermochemical Conversion of Biomass to Liquid Fuels and Chemicals* **2010**, 73−130.

(12) Fiddler, W.; Parker, W. E.; Wasserman, A. E.; Doerr, R. C. Thermal Decomposition of Ferulic Acid. *J. Agric. Food Chem.* **1967**, *15* (5), 757−761.

(13) Werner, K.; Pommer, L.; Broström, M. Thermal Decomposition of Hemicelluloses. *J. Anal. Appl. Pyrolysis* **2014**, *110*, 130−137.

(14) Wang, S.; Ru, B.; Dai, G.; Sun, W.; Qiu, K.; Zhou, J. Pyrolysis Mechanism Study of Minimally Damaged Hemicellulose Polymers Isolated from Agricultural Waste Straw Samples. *Bioresour. Technol.* **2015**, *190*, 211−218.

(15) Lv, G.; Shu-Bin, W.; Lou, R. Kinetic Study of the Thermal Decomposition of Hemicellulose Isolated from Corn Stalk. *BioResources* **2010**, *5* (2), 1281−1291.

(16) Peng, Y. Y.; Wu, S. B. Fast Pyrolysis Characteristics of Sugarcane Bagasse Hemicellulose. *Cellul. Chem. Technol.* **2011**, *45* (9−10), 605−612.

(17) Wang, S.; Ru, B.; Lin, H.; Sun, W. Pyrolysis Behaviors of Four O-Acetyl-Preserved Hemicelluloses Isolated from Hardwoods and Softwoods. *Fuel* **2015**, *150*, 243−251.

(18) Chen, D.; Zhou, J.; Zhang, Q.; Zhu, X. Evaluation Methods and Research Progresses in Bio-Oil Storage Stability. *Renewable Sustainable Energy Rev.* **2014**, *40*, 69−79.

(19) Park, L. K. E.; Liu, J.; Yiacoumi, S.; Borole, A. P.; Tsouris, C. Contribution of Acidic Components to the Total Acid Number (TAN) of Bio-Oil. *Fuel* **2017**, *200*, 171−181.

(20) Knothe, G. Analyzing Biodiesel: Standards and Other Methods. *J. Am. Oil Chem. Soc.* **2006**, *83* (10), 823−833.

(21) Laesecke, J.; Ellis, N.; Kirchen, P. Production, Analysis and Combustion Characterization of Biomass Fast Pyrolysis Oil - Biodiesel Blends for Use in Diesel Engines. *Fuel* **2017**, *199*, 346−357.

(22) Greenhalf, C. E.; Nowakowski, D. J.; Harms, a. B.; Titiloye, J. O.; Bridgwater, a. V. A Comparative Study of Straw, Perennial Grasses

and Hardwoods in Terms of Fast Pyrolysis Products. *Fuel* **2013**, *108*, 216−230.
(23) Frisch, M. J.; et al. *Gaussian 09*, Revision D.01; Gaussian, Inc.: Wallingford, CT, 2009.
(24) Becke, A. D. Density-Functional Exchange-Energy Approximation with Correct Asymptotic Behavior. *Phys. Rev. A: At., Mol., Opt. Phys.* **1988**, *38* (6), 3098−3100.
(25) Frisch, M. J.; Trucks, G. W.; Schlegel, H. B.; Scuseria, G. E.; Robb, M. A.; Cheeseman, J. R.; Scalmani, G.; Barone, V.; et al. *Gaussian 09*, Revision D.02. Gaussian, Inc: Wallingford, CT 2009.
(26) Eckart, C. The Penetration of a Potential Barrier by Electrons. *Phys. Rev.* **1930**, *35* (11), 1303−1309.
(27) Lizardo-Huerta, J. C.; Sirjean, B.; Bounaceur, R.; Fournet, R. Intramolecular Effects on the Kinetics of Unimolecular Reactions of β-HOROO and HOQOOH Radicals. *Phys. Chem. Chem. Phys.* **2016**, *18* (17), 12231−12251.
(28) Pfaendtner, J.; Yu, X.; Broadbelt, L. J. The 1-D Hindered Rotor Approximation. *Theor. Chem. Acc.* **2007**, *118* (5−6), 881−898.
(29) Pauly, M.; Keegstra, K. Cell-Wall Carbohydrates and Their Modification as a Resource for Biofuels. *Plant J.* **2008**, *54* (4), 559−568.
(30) Usino, D. O.; Supriyanto; Ylitervo, P.; Pettersson, A.; Richards, T. Influence of Temperature and Time on Initial Pyrolysis of Cellulose and Xylan. *J. Anal. Appl. Pyrolysis* **2020**, *147*, 104782.
(31) Wang, S.; Ru, B.; Dai, G.; Sun, W.; Qiu, K.; Zhou, J. Pyrolysis Mechanism Study of Minimally Damaged Hemicellulose Polymers Isolated from Agricultural Waste Straw Samples. *Bioresour. Technol.* **2015**, *190*, 211−218.
(32) Paine, J. B.; Pithawalla, Y. B.; Naworal, J. D.; Thomas, C. E. Carbohydrate Pyrolysis Mechanisms from Isotopic Labeling Part 1: The Pyrolysis of Glycerin: Discovery of Competing Fragmentation Mechanisms Affording Acetaldehyde and Formaldehyde and the Implications for Carbohydrate Pyrolysis. *J. Anal. Appl. Pyrolysis* **2007**, *80*, 297−311.
(33) Paine, J. B.; Pithawalla, Y. B.; Naworal, J. D. Carbohydrate Pyrolysis Mechanisms from Isotopic Labeling Part 2. The Pyrolysis of D-Glucose: General Disconnective Analysis and the Formation of C1 and C2 Carbonyl Compounds by Electrocyclic Fragmentation Mechanisms. *J. Anal. Appl. Pyrolysis* **2008**, *82*, 10−41.
(34) Paine, J. B.; Pithawalla, Y. B.; Naworal, J. D. Carbohydrate Pyrolysis Mechanisms from Isotopic Labeling Part 3. The Pyrolysis of D-Glucose: Formation of C3 and C4 Carbonyl Compounds and a Cyclopentenedione Isomer by Electrocyclic Fragmentation Mechanisms. *J. Anal. Appl. Pyrolysis* **2008**, *82*, 42−69.
(35) Paine, J. B.; Pithawalla, Y. B.; Naworal, J. D. Carbohydrate Pyrolysis Mechanisms from Isotopic Labeling Part 4. The Pyrolysis of D-Glucose: The Formation of Furans. *J. Anal. Appl. Pyrolysis* **2008**, *83*, 37−63.
(36) Nimlos, M. R.; Blanksby, S. J.; Qian, X.; Himmel, M. E.; Johnson, D. K. Mechanisms of Glycerol Dehydration. *J. Phys. Chem. A* **2006**, *110* (18), 6145−6156.
(37) Shen, D. K.; Gu, S.; Bridgwater, A. V. Study on the Pyrolytic Behaviour of Xylan-Based Hemicellulose Using TG-FTIR and Py-GC-FTIR. *J. Anal. Appl. Pyrolysis* **2010**, *87* (2), 199−206.
(38) Nagy, P. I.; Dunn, W. J.; Alagona, G.; Ghio, C. Theoretical Calculations on 1,2-Ethanediol. 2. Equilibrium of the Gauche Conformers with and without an Intramolecular Hydrogen Bond in Aqueous Solution. *J. Am. Chem. Soc.* **1992**, *114* (12), 4752−4758.
(39) Branca, C.; Giudicianni, P.; Di Blasi, C. GC/MS Characterization of Liquids Generated from Low-Temperature Pyrolysis of Wood. *Ind. Eng. Chem. Res.* **2003**, *42* (14), 3190−3202.
(40) Nowakowski, D. J.; Jones, J. M. Uncatalysed and Potassium-Catalysed Pyrolysis of the Cell-Wall Constituents of Biomass and Their Model Compounds. *J. Anal. Appl. Pyrolysis* **2008**, *83* (1), 12−25.
(41) Beyer, M. K. The Mechanical Strength of a Covalent Bond Calculated by Density Functional Theory. *J. Chem. Phys.* **2000**, *112* (2000), 7307−7312.
(42) Verma, A. M.; Agrawal, K.; Kawale, H. D.; Kishore, N. Quantum Chemical Study on Gas Phase Decomposition of Ferulic Acid. *Mol. Phys.* **2018**, *116* (14), 1895−1907.
(43) Laidler, K. J. *Chemical Kinetics*; Pearson, 1987.

https://dx.doi.org/10.1021/acs.energyfuels.0c02901
Energy Fuels XXXX, XXX, XXX−XXX